Chandra HETG Observations of the Colliding Stellar Wind System WR 147

Svetozar A. Zhekov[1,3] and Sangwook Park[2]

ABSTRACT

We present an extended analysis of deep *Chandra* HETG observations of the WR+OB binary system WR 147 that was resolved into a double X-ray source (Zhekov & Park 2010). Our analysis of the profiles of strong emission lines shows that their centroids are blue-shifted in the spectrum of the northern X-ray source. We find no suppressed forbidden line in the He-like triplets which indicates that the X-ray emitting region is not located near enough to the stars in the binary system to be significantly affected by their UV radiation. The most likely physical picture that emerges from the entire set of HETG data suggests that the northern X-ray source can be associated with the colliding stellar wind region in the wide WR+OB binary system, while the X-rays of its southern counterpart, the WN8 star, are result from stellar wind shocking onto a close companion (a hypothesized third star in the system).

Subject headings: stars: individual (WR 147) — stars: Wolf-Rayet — X-rays: stars — shock waves

1. Introduction

WR+OB binaries are the brightest X-ray sources amongst the Wolf-Rayet (WR) stars (Pollock 1987). Their enhanced emission originates from the interaction region of the winds of the two massive stars (Prilutskii & Usov 1976; Cherepashchuk 1976). Since the winds are highly supersonic, the interaction region is bounded by two shocks each compressing the stellar wind of the WR or OB star, and a contact discontinuity surface separating their shocked plasmas (for the first hydrodynamic models see Lebedev & Myasnikov 1990; Luo et al. 1990;

[1]JILA, University of Colorado, Boulder, CO 80309-0440, USA; zhekovs@colorado.edu

[2]Department of Astronomy and Astrophysics, Pennsylvania State University, 525 Davey Laboratory, University Park, PA 16802, USA; park@astro.psu.edu

[3]On leave from Space Research Institute, Sofia, Bulgaria

Stevens et al. 1992; Myasnikov & Zhekov 1991, 1993). Given the wind velocities (typical values of 1,000-3,000 km s^{-1}), the postshock temperatures are in the keV range, and most of the plasma emission is thus in X-rays. If the shocks are adiabatic, the X-ray luminosity of the colliding stellar winds (CSW) is proportional to the square of the mass-loss rate ($\dot{M}$) and inversely to the binary separation (D): $L_X \propto \dot{M}^2 V_{wind}^{-3.2} D^{-1}$ (see the references above for discussion). From this follows: (i) the shocked WR wind dominates the X-ray emission from CSW in WR+OB binaries due to its much more massive wind ($\dot{M}$ of a WR star is about an order of magnitude higher than that of an O star); (ii) by the same argument, a WR+OB binary will be more luminous in X-rays than an OB+OB binary, with similar wind velocities and binary separation.

On the other hand, CSWs in close and wide binaries have quite different behavior. While in the former, shocks are radiative and thus the interaction region is subject to instabilities (e.g., Stevens et al. 1992; Myasnikov et al. 1998; Walder & Folini 2000), the shocks are adiabatic in the latter and the effects of thermal conduction might also be important (Myasnikov & Zhekov 1998). Moreover, the effects of electron-ion temperature equilibration behind the shocks (Zhekov & Skinner 2000) and non-equilibrium ionization (Zhekov 2007) can influence the X-ray emission from CSWs.

A difference between CSWs in close and wide WR binaries is also seen in radio, and as a rule non-thermal radio (NTR) sources are associated with the wide binary systems (Dougherty & Williams 2000). The strong shocks are the likely place for accelerating relativistic particles, and the CSWs in wide binaries offer good conditions for this mechanism to operate efficiently since the shocks are located relatively far from the optically bright sources (the stars) and thus the inverse Compton losses are minimal (for the first detailed models of NTR emission from CSWs see Dougherty et al. 2003; Pittard et al. 2006).

It is therefore seen that the CSWs in stellar binaries are an ideal laboratory for studying the wealth of physical processes related to strong shocks. With the launch of the modern X-ray observatories providing high spectral and spatial resolution observations (*Chandra*, *XMM-Newton*), a new window has opened for gathering detailed information about this exciting phenomenon. By confronting theoretical models of CSWs with observations, we can rigorously test them, and thus improve our understanding of the underlying physics. For such a goal, it is necessary to have an object which is bright enough in X-rays, it is a strong non-thermal radio source and it is relatively close to us. Thus, its radio-to-X-ray emission might be spatially resolved and provide us with detailed information about the CSW region and the stars in the binary system. Because the two components in the binary system can be separated, WR 147 is unique amongst the massive WR+OB binaries and offers a rare opportunity for studying the CSW-binary phenomenon in its entirety.

We report here results from our analysis of deep *Chandra* HETG observations of the CSW binary WR 147 . Zhekov & Park (2010) presented the first part of our study based on the zeroth-order HETG data whose most important result is that the X-ray emission from WR 147 was resolved into two sources. This paper is organized as follows. We give basic information about the WR+OB binary WR 147 in Section 2. In Section 3, we briefly review the *Chandra* HETG observations. In Section 4, we present the results from analysis of strong X-ray emission lines. In Section 5, we discuss the origin of X-rays in the two X-ray components of WR 147 . In Section 6, we report results from the global spectral models. In Section 7, we discuss our results and we list our conclusions in Section 8.

2. The Wolf-Rayet Binary WR 147

The Wolf-Rayet star WR 147 (WR+OB; van der Hucht 2001) is a classical example of colliding wind binary at a distance of 630 ± 70 pc (Churchwell et al. 1992). High-resolution radio observations resolved its emission into two components: a southern thermal source, WR 147S (the WN8 star in the system), and a northern non-thermal source, WR 147N (Abbott et al. 1986; Moran et al. 1989; Churchwell et al. 1992; Contreras et al. 1996; Williams et al. 1997; Skinner et al. 1999) with separation of $\sim 0\farcs57$. The binary system was spatially resolved both in infrared and optical to have a separation of $\sim 0\farcs64$ (Williams et al. 1997; Niemela et al. 1998) which at the distance to this object corresponds to projected (or minimum) binary separation of 403 ± 13 au. While the spectral type of the WR star in the binary is well defined (WN8h; van der Hucht 2001), that of the OB companion is not well constrained. From spatially resolved near-infrared and optical photometry, the spectral type of the latter was estimated correspondingly as a B0.5V (Williams et al. 1997) and O8-9 V-III (Niemela et al. 1998). And Lèpine et al. (2001) classified it as a O5-7 I-II from spatially resolved spectra, but in the red optical domain.

Due to the high extinction towards WR 147 ($A_V = 10.45$; $A_V = A_v/1.11$; $A_v = 11.6$; van der Hucht 2001), the WR wind parameters, $\dot{M} = 4\times10^{-5}$ $M_\odot$ yr^{-1} ; $V_{wind} = 950$ km s^{-1} , were derived from radio and NIR observations (Skinner et al. 1999; Morris et al. 2000). For consistency with the previous works (Skinner et al. 1999; Skinner et al. 2007; Zhekov 2007), we adopt $\dot{M} = 6.6 \times 10^{-7}$ $M_\odot$ yr^{-1} ; $V_{wind} = 1600$ km s^{-1} for the stellar wind parameters of the OB companion.

The previous X-ray observations of WR 147 have revealed the presence of thermal emission from high temperature plasma: kT ≥ 0.5 keV (*Einstein* observatory; Caillault et al. 1985); kT ≈ 1 keV (*ASCA*; Skinner et al. 1999); kT $= 2.7$ keV (*XMM-Newton*; Skinner et al. 2007) as the *XMM-Newton* observations detected the Fe K_α complex at 6.67 keV which is a

clear sign of thermal X-rays even at high energies. Note that the temperature change simply reflects the improving quality of the X-ray data over the years.

The observations with *Chandra* High-Resolution Camera (having low photon statistics, ~ 148 source counts, and no spectral information) found indications that the X-ray emitting region in WR 147 might be extended and it peaks north from the WN8 star although a deeper X-ray image was needed to determine the degree of spatial extent (Pittard et al. 2002).

The recent high resolution *Chandra* observations resolved the X-ray emission from WR 147 into two sources, WR 147N and WR 147S , with a spatial separation of $\approx 0\farcs60$ (Zhekov & Park 2010). The corresponding analysis of undispersed spectra showed that WR 147N and WR 147S have different global characteristics as the latter being more absorbed and having higher plasma temperature: $N_H = 2.28\,[2.08 - 2.57] \times 10^{22}$ cm^{-2}; kT $= 1.78\,[1.52 - 1.98]$ keV for WR 147N ; $N_H = 3.83\,[3.51 - 4.20] \times 10^{22}$ cm^{-2}; kT $= 2.36\,[2.12 - 2.56]$ keV for WR 147S . It is worth noting that the absorption towards WR 147N almost perfectly corresponds to the optical extinction of WR 147 if the Gorenstein (1975) conversion is used.

3. Observations and Data Reduction

WR 147 was observed with *Chandra* in the configuration HETG-ACIS-S in eight consecutive runs (Chandra ObsIds: 9941, 9942, 10675, 10676, 10677, 10678, 10893 and 10897) in the period 2009 Mar 28 - Apr 10, providing a total effective exposure of 286 ksec. The roll angle was between 75° and 82°: therefore, the dispersion axis was aligned approximately with the position angle of the binary system WR 147 as derived in the optical (P.A. $= 350° \pm 2$; Niemela et al. 1998). The instrument configuration was such that the *negative* first-order MEG/HEG arms were pointing to north. By default, the pixel randomization is switched off in grating data.

As reported in Zhekov & Park (2010), the X-ray emission from WR 147 was spatially resolved into a northern, WR 147N , and a southern counterpart, WR 147S (the WN8 star in the binary). Thus, following the Science Threads for Grating Spectroscopy in the CIAO 4.1.2 [1] data analysis software, the positive and negative first-order MEG/HEG spectra for each of the eight observations were extracted centered on the WR 147S position on the sky. The *Chandra* calibration database CALDB v.4.1.3 was used in this analysis. The resultant

[1]Chandra Interactive Analysis of Observations (CIAO), http://cxc.harvard.edu/ciao/

spectra were merged into one spectrum each for the positive and negative MEG/HEG arms with respective total counts of 2742 (MEG+1), 2396 (MEG−1), 1438 (HEG+1) and 1606 (HEG−1). The zeroth-order data were discussed in Zhekov & Park (2010) and we only mention that the total number of zero order counts in the WR 147N and WR 147S spectra were 2158 and 5108, respectively. We note that terms WR 147 and WR 147N+S will be used throughout the text to refer to the total X-ray emission (and spectra) of the studied WR+OB binary system.

For the spectral analysis in this study, we made use of standard as well as custom models in version 11.3.2 of XSPEC (Arnaud 1996).

4. Spectral Lines

The X-ray emission from WR 147 is dominated by WR 147S (Zhekov & Park 2010) and the presence of another source (WR 147N) at $\sim 0\farcs6 - 0\farcs64$ will cause the emission line profiles to be 'blurred' since the WR 147S - WR 147N orientation on the sky is approximately along the South-North direction, that is parallel to the dispersion axis. If there were no line shifts in the WR 147N emission, the line centroids in the total WR 147 spectrum would correspondingly show *blue shifts* in the positive and *red shifts* in the negative arms of the MEG/HEG spectra and their values will be the same ($|z(+1)| = |z(-1)|$). If the WR 147N emission was intrinsically blue-shifted, this would result in larger line shifts in the MEG/HEG(+1) than in the MEG/HEG(−1) for each spectral line ($|z(+1)| > |z(-1)|$). The result would be just the opposite ($|z(+1)| < |z(-1)|$), if the WR 147N spectrum was red-shifted.

For each spectral line, we fitted all four spectra, MEG($+1/-1$) and HEG($+1/-1$), simultaneously as they were re-binned every two bins to improve the photon statistics. For the S XV and Si XIII He-like triplets, we fitted a sum of three Gaussians and a constant continuum. The centers of the triplet components were held fixed according to the *Chandra* atomic data base[2] and all components share the same line width and line shifts. Similarly, we fitted the Si XIV and Mg XII H-like doublets but the component intensities were fixed through their atomic data values. Figure 1 shows the results for the line shifts of prominent lines in the X-ray spectrum of WR 147 . We see that all the lines are blue-shifted in the MEG/HEG(+1) and red-shifted in the MEG/HEG(−1) spectra and $|z(+1)| > |z(-1)|$. Thus, the results indicate *blue-shifted* X-ray emission from WR 147N . And, we note that we do not find suppressed forbidden line in the He-like triplets.

[2]For ATOMDB, see http://cxc.harvard.edu/atomdb/

Motivated by these results, we developed a custom model for XSPEC to fit the line profiles that consist of line emission from two sources with an 'offset', Δ, for the line center of the second one. We note that for the instrument configuration of our observations (§ 3) and since the second source (WR 147N) is located north from WR 147S its spectral lines will get a red shift in the negative first-order spectra and a blue shift in the positive first-order spectra that correspond to the spatial offset Δ. But for MEG and HEG this line shift will be different in units of wavelength due to their different spectral resolution ($\Delta_{MEG} = 2\Delta_{HEG}$). For each source, the profiles of the spectral line doublets and triplets were treated as described above. We fitted this model to the line profiles of the H-like doublets of Mg XII and Si XIV as well as of the He-like triplets of Si XIII and S XV again simultaneously for the four first-order spectra. The fit results are given in Table 1 and individual line profiles are shown in Fig. 2.

From the fit results we see that the line profiles in the spectrum of WR 147S are broader than those in WR 147N : bulk gas velocities (FWHM) with a typical value of $\approx$ 1000 km s^{-1} are present in the former while the line widths indicate slower gas motion ($<$ 1000 km s^{-1}) for the latter. This may be a sign of different X-ray production mechanisms and we will return to this issue in § 5. An important feature of these mechanisms is that we do not find suppressed forbidden line in the He-like triplets which means that the X-ray emission plasma has relatively low density and/or the hot plasma regions both in WR 147S and WR 147N are located far enough from strong UV sources.

Perhaps the two most interesting fit results are related to WR 147N alone. First, we see that despite their relatively large errors the centroids of *all* the studied lines are *blue-shifted* as anticipated from the preliminary analysis of the line profiles (see above). Second, the values for the spatial 'offset' between WR 147N and WR 147S are consistent between different spectral lines. Interestingly, the average value from all four spectral lines, $\bar{\Delta} = 0\farcs603^{+0.10}_{-0.08}$, is in a very good correspondence with the source separation measured directly from the deconvolved (1.0 - 2.0 keV) zeroth-order image of WR 147 (Zhekov & Park 2010). This is a very important internal cross-check for the HETG results and another nice illustration of the superior spatial and spectral resolution of the *Chandra* observatory.

Finally, for the analysis here we assumed that the spectral lines of WR 147S are not shifted and the reason was that the fits are too complicated already, thus, an extra free parameter in the fits cannot be constrained well due to the quality of the data. But we note that we derived results generally consistent with zero line shifts if we let this parameter vary (the average value from the line shifts of the prominent line complexes in the spectrum of WR 147S is -96$^{+75}_{-76}$ km s^{-1}).

5. The Origin of X-ray Emission from WR 147

Thanks to its superior spatial resolution, *Chandra* resolved the CSW binary WR 147 into a double X-ray source. The different spectral characteristics (plasma temperature and X-ray absorption) as deduced from the analysis of the undispersed spectra of both components (Zhekov & Park 2010; see also § 2) as well as the results from the fits to spectral line profiles in the first-order spectra (§ 4) likely point to different emission mechanisms responsible for the X-ray emission from WR 147N and WR 147S .

5.1. X-rays from WR 147N

Since WR 147 is a spatially resolved radio source with thermal and non-thermal components, all the analyses of its X-ray emission before the *Chandra* observations have assumed that the colliding stellar winds are responsible for the total X-ray emission from this WR+OB binary. We now know that the physical picture is more complex and at least two components are contributing to the X-ray emission of the WR 147 system. Thus, only the northern source, WR 147N , can be associated with the CSW region in this binary system (Zhekov & Park 2010). But, the presence of another massive star (the OB companion in the binary) in vicinity of WR 147N requires a more careful look into such an identification.

We recall that Zhekov & Park (2010) found that the CSW model with nominal wind parameters for WR 147 perfectly matches the shape of the X-ray spectrum of WR 147N . They also reported a correspondence between the location of WR 147N in X-rays and WR 147N in the radio, and the latter is definitely associated with the CSW region in WR 147 (Contreras & Rodriguez 1999). We could prove that WR 147N is located in the CSW region of the binary system if the X-ray separation between WR 147N and WR 147S is smaller than the value derived from the optical and NIR imaging. This would indicate that the northern X-ray source is detached from the surface of the OB companion. However, the values derived from the X-ray analysis do not provide solid evidence for that due to their uncertainties (see § 4 and Table 1).

Extended emission in WR 147N would support that this source is the CSW region, but we see no extended X-ray emission in the HETG zeroth-order image that might have morphology similar to that of the extended non-thermal radio emission in WR 147N (Contreras & Rodriguez 1999). A reason for that could be the limited photon statistics in soft X-rays (only ~ 700 counts in the 1-2 keV band) and we note that soft X-rays originate downstream from the shocks that is in the 'outskirts' of the CSW region. Thus, future X-ray observations that provide images with higher quality may help us establish with certainty the morphology

of WR 147N which in turn will be very helpful in resolving the issue about the proper identification of this X-ray source.

On the other hand, the massive OB stars are X-ray sources and could it be that the northern X-ray source, WR 147N , is in fact the OB companion in this wide binary system? In general, this might well be the case but there are some pieces of indirect evidence that make such an identification more unlikely. For example, the plasma temperature in WR 147N is relatively high (kT = 1.78 keV; § 2) while OB stars are in general 'soft' X-ray sources with temperatures below 1 keV (e.g., Wojdowski & Schulz 2005; Zhekov & Palla 2007; see also §4.1.2 and §4.3 in the review paper of Güdel & Nazé 2009 and the references therein). As a reference case, we ran XSPEC simulations having exposure of 286 ksec for a 'soft' X-ray source with kT = 0.6 keV, $L_X(0.5-10\ \mathrm{keV}) = 10^{31}$ ergs s^{-1} and $N_H = 2.3 \times 10^{22}$ cm^{-2} (typical for WR 147N), using the ancillary response functions from our zeroth-order HETG observation. We found 30-40 source counts or $< 2\%$ from the total zero order counts of WR 147N . This indicates that a 'soft' X-ray source will likely have a small contribution to the total emission from WR 147N . But, exceptions could be the rare hot magnetic objects like the massive O star θ^1 Ori C and the B star τ Sco whose spectra show signs of considerably hotter plasma (Schulz et al. 2003; Gagné et al. 2005; Cohen et al. 2003). The X-ray production mechanism that is believed to operate in such objects is that of magnetically confined wind shocks (MCWS, e.g., Babel & Montmerle 1997; ud-Doula & Owocki 2002). This model suggests that the X-ray emission mostly originates in regions very close to the stellar surface, thus, due to the strong stellar UV emission the forbidden line can likely be suppressed even in the He-like triplets as Si XIII and S XV. In fact, this is the case in the classical MCWS object θ^1 Ori C (Gagné et al. 2005) and similar indications are found for τ Sco (Cohen et al. 2003). Opposite to this, we do not find suppressed forbidden line in the Si XIII and S XV He-like triplets in the X-ray spectrum of WR 147N (§ 4) which indicates that these lines are formed in regions far from the surface of the OB companion. It is also worth noting that because of the expected decay of the magnetic field strength with the age of a massive star, the MCWS mechanism is associated only with young massive stars (age $\leq$ 1 Myr; Schulz et al. 2003). But, the age of the OB star in the wide WR+OB binary system WR 147 must be larger than 1-2 Myr as indicated by the presence of a WR star in the system.

From all this, a physical picture in which WR 147N resides in the CSW region seems more realistic than assuming that WR 147N is associated with the OB companion in the massive binary system WR 147 . However, we should keep in mind that the CSW model with nominal wind parameters for WR 147 overestimates the observed WR 147N luminosity by a factor of ~ 16 (Zhekov & Park 2010), a discrepancy that must find reasonable explanation in the CSW scenario. We will discuss possible solutions to this problem in § 7.

5.2. WR 147S : Unusual X-ray Source

The X-ray detection of the WN8 star in WR 147 and its brightness make it unusual amongst the WR stars of the same subtype. As shown by Skinner et al. (2010), single WN7-9 stars are very weak X-ray sources. And, the X-ray emission of WR 147S is quite hard as the analysis of its undispersed spectrum indicated (kT = 2.36 keV).

Skinner et al. (2002a,b, 2010) discussed in some detail possible mechanisms for X-ray production in WN stars, which include: instability-driven wind shocks; magnetically confined wind shocks; wind accretion shocks; colliding wind shocks (including the case of stellar wind shocking onto a close companion); non-thermal X-ray emission. We note that none of these mechanisms finds solid observational support for the moment and each of them has its own limitations and caveats. We recall that instability-driven wind shocks are supposed to be soft X-ray emitters which is not the case with WR 147S . Accretion wind shocks result in a relatively high X-ray luminosity ($\sim 10^{36-37}$ ergs s^{-1}) and the observed value is short by 3-4 orders of magnitude. As discussed above (§ 5.1), in the magnetically confined wind shock picture X-rays form close to the stellar surface which results in a suppressed forbidden line even in He-like triplets as Si XIII and S XV due to the strong stellar UV emission. Opposite to this, we find no indications for such a suppression in the spectrum of WR 147S (§ 4). And, the X-ray spectrum of WR 147S definitely has a thermal origin as indicated by the presence of various spectral lines that originate in thermal plasma and this is also the case at high energies. Skinner et al. (2007) detected a Fe XXV K-line at 6.67 keV in the *XMM-Newton* spectra of WR 147 and the zeroth-order HETG data undoubtedly showed that this line is associated with WR 147S , the WN8 star in the binary system (Zhekov & Park 2010).

But, the case of X-rays from the stellar wind shocking onto a close companion seems to find some support from our deep *Chandra* observations that span an almost two-week period. Figure 3 shows the light curve of WR 147 in different energy bands. Obviously, a long-term variability is present in the data with a tentative period of 15-20 days. This variability is well established at high energies, thus, it should be associated with WR 147S which dominates the X-ray emission at E > 3 keV. We fitted the light curve with two models: a constant flux and a simple sinusoidal curve. The values for the reduced χ^2 for various fits are: $\chi^2(0.3-10\ keV) = 1.55$ (sine) and 3.79 (const); $\chi^2(0.3-2\ keV = 1.63$ (sine) and 1.14 (const); $\chi^2(3-10\ keV) = 0.49$ (sine) and 4.49 (const). The formal goodness of fit is: 0.20 (sine) and 0.0009 (const) for the (0.3-10 keV) LC; 0.18 (sine) and 0.34 (const) for the (0.3-2 keV) LC; 0.69 (sine) and 0.0002 (const) for the (3-10 keV) LC. The corresponding periods are: P(0.3-10 keV)= 17.61 ± 3.74 days; P(3-10 keV)= 15.48 ± 1.91 days. The amplitudes of the variability with respect to the constant flux are: 7% in (0.3-10 keV); 13% in (3-10 keV).

Thus, if the X-rays in WR 147S originate from stellar wind shocking onto a close compan-

ion, the observed variability might simply correspond to the orbital period of the companion star. The changes in the X-ray emission could be a result from the ellipticity of the orbit (variable emission measure) and/or they may be due to a variable X-ray absorption depending on the inclination angle of the orbit. Unfortunately, the quality of the individual spectra in the HETG data set (zeroth and first order spectra) does not allow us address these issues. We only note that for an adopted value of 15.48 days for the orbital period and a total mass of the system of 20 $M_\odot$, the Kepler's third law ($a = 0.01952 P_d^{2/3} [M/M_\odot]^{1/3}$ au; P_d is the orbital period in days; M is the total mass) gives $a = 0.33$ au for the semi-major axis of the orbit. For a distance of 630 pc to WR 147 (Churchwell et al. 1992), the separation between the WN8 star and the normal star companion will be $\approx 0\farcs0005$. Being that close to a luminous hot star makes it highly unlikely for such an object be detected by imaging techniques. On the other hand, we can speculate that this variable X-ray source provides extra ionizing photons that are capable of changing the population in highly ionization stages of elements as carbon, nitrogen and oxygen. Given the spectral subtype of the WR star in WR 147 (WN8), we can propose that variability in the profiles of NIV and NV lines can be expected in the optical with a periodicity as seen in X-rays, an effect similar to the Hatchett-McCray effect in massive X-ray binaries (Hatchett & McCray 1977).

6. Global Spectral Models

A systematic approach to modeling the total X-ray spectrum of WR 147N+S would be to fit the entire observed spectrum using a reasonable physical model. We note that the HETG first-order spectra represent the total (combined) X-ray emission of the two X-ray sources WR 147N and WR 147S . As discussed in § 5.1, the most realistic assumption for the X-rays in WR 147N is that they originate from the CSW region in the binary system. Thus, we explore this picture in some detail. On the other hand, the origin of the X-ray emission in WR 147S is not well constrained and we consider two limiting cases: a distribution of adiabatic shocks and a distribution of equilibrium plasma.

For the spectrum of WR 147N , we adopted the CSW model with non-equilibrium ionization by Zhekov (2007) and we made a new version for XSPEC that explicitly takes into account the line broadening (bulk gas velocities) from the hydrodynamic CSW model. An important feature of the new version is that it includes a spatial 'offset' for the CSW source with respect to a near by source which is the case with the HETG first-order spectra of WR 147N . Moreover, to get realistic line profiles we need to know the position of the observer (line of sight) with respect to the CSW region (its axis of symmetry). This requires two more model parameters: the inclination angle, i (the angle between the line of sight

and the orbital axis) and the azimuthal angle, ω (defining the position of the observer in the orbital plane). We recall that the CSW model by Zhekov (2007) makes use of the hydrodynamic model of Myasnikov & Zhekov (1993) which adopts a convention that the O star in the binary system is located at the origin of the coordinate system. Panel (a) in Fig. 4 shows a schematic diagram of the wind interaction of two spherically symmetric stellar winds in a WR+OB binary.

Since the CSW spectral calculations require 3D integration, it is not feasible to fit for the values of the orbital inclination and azimuthal angle of the observer's line of sight. Some information about these parameters comes from the analysis of the spectral line profiles (§ 4). We recall that blue-shifted lines were found in the spectrum of WR 147N . This indicates that the CSW region is inclined towards the observer. That is, the CSW region is located between the observer and the WN8 star (WR 147S).

To explore this in detail, we have run a grid of CSW models for $\omega \in [90, 180]$. One should keep in mind that due to the axial symmetry of the CSW region, the line shifts (and line profiles) from the CSW region are the same for $\omega \in [90, 180]$ and $\omega = 360 - \omega$, and a given value of i. To be as close as possible to the observational situation, we carried out the CSW spectral simulations in XSPEC using the ancillary response functions from our HETG observations. We fitted the spectral lines in simulated CSW spectra in a similar way as for the real data analysis: using a sum of two and three Gaussians for the lines of H-like doublets and He-like triplets, respectively.

Panel (b) in Fig. 4 shows the isolines for the observed line shifts of S XV, Si XIV, Si XIII and Mg XII (from Table 1) in the (i, ω) parameter space from our model calculations. From this in conjunction with the result about the orientation of the WR-OB binary axis on the sky (Niemela et al. 1998), we conclude that the orbital inclination is smaller than 60° with an average value of 30°: the isolines cluster around $20° - 40°$. The upper limit of the inclination angle comes from the largest possible value from the 1σ-error on the line shift of acceptably well constrained data: in this case it is from the Si XIII triplet and is shown with a solid curve in panel (b) of Fig. 4. We note that the value for the 1σ-error of the S XV triplet is beyond this limit but this is likely due to the poorer quality of the data for this line and the fact that the contribution from the CSW region is small (Table 1). This prevents having a tighter constraint (smaller uncertainties) on its line shift although the derived value is consistent with those for the other lines in our analysis. From the values of the observed position angle of the WR-OB star axis on the sky (Niemela et al. 1998), we derive a value for the azimuthal angle $\omega = 170° - 174°$ (see Fig. 4).

Contreras & Rodriguez (1999) derived a $(45° \pm 15°)$ range of possible inclination angles for the WR 147 system from the analysis of the morphology of the non-thermal radio source

WR 147N . Thus, in the framework of the CSW picture, the results from the HETG observations are generally consistent with those from the radio observations of WR 147 . But, we now obtain an additional piece of information: the CSW region is inclined towards the observer. Blue-shifted lines were detected, so the CSW region lies between the observer and the WN8 star.

Our global spectral model consists of two components: a CSW NEI model representing the X-ray emission from WR 147N and a thermal plasma component for the X-ray spectrum of WR 147S . In accord with the spectral analysis of Zhekov & Park (2010), both spectra are subject to the same X-ray absorption from the interstellar matter (ISM; $\mathrm{N}_H = 2.3 \times 10^{22}$ cm^{-2}) and there is an excess X-ray absorption of the WR 147S spectrum which we assume is due to the WN8 wind. Since the value for the ISM absorption corresponds well to the optical extinction to WR 147 , we keep its value fixed in this analysis. The WN-wind absorption is a free parameter and for that purpose we adopted the cold wind approximation by making use of the *vphabs* model in XSPEC. This allows us to impose the same set of chemical abundances on the hot X-ray emitting plasma and the wind absorber. We recall that the CSW model at hand takes into account that the shocked OB-star wind has solar abundances while the shocked WN wind has a different set of abundances that can be adjusted in the fitting process. Thus, the CSW model and the model for the X-ray emission from WR 147S share their abundances. For consistency with the previous studies we adopted the same set of WN abundances (see Skinner et al. 2007; Zhekov 2007) as only the values for Ne, Mg, Si, S, Ar, Ca and Fe were allowed to vary while those for the other elements were held fixed in the fits.

The CSW model uses nominal stellar wind parameters ($\mathrm{V}_{WR} = 950$ km s^{-1}, $\dot{M}_{WR} = 4 \times 10^{-5}$ $\mathrm{M}_\odot$ yr^{-1}; $\mathrm{V}_O = 1600$ km s^{-1}, $\dot{M}_O = 6.6 \times 10^{-7}$ $\mathrm{M}_\odot$ yr^{-1}; $[\dot{M}_O V_O / \dot{M}_{WR} V_{WR}] = 0.028$) and a value of 403 au for the projected binary separation (§ 2). But the mass-loss values for the winds of both stars were reduced by a factor of 4 to correct for the CSW luminosity discrepancy revealed from the analysis of the undispersed spectra (Zhekov & Park 2010). The orbital inclination and azimuthal angle were held fixed to $i = 30°$ and $\omega = 171°$. Also, a spatial offset with a fixed value of $\Delta = 0\farcs603$ (§ 4) was adopted for the CSW X-ray source (WR 147N).

As mentioned above, we adopted thermal plasma models for the X-ray spectrum of WR 147S that consider two limiting cases. The first case is a distribution of adiabatic shocks with non-equilibrium ionization effects (NEI shocks) and we made use of our custom model for XSPEC which was successfully used in the analysis of the X-ray spectra of SNR 1987A (e.g. Zhekov et al. 2009 and references therein). The second one considers a distribution of emission measure of thermal plasma in ionization equilibrium (CIE plasma) and we adopted our custom model which is similar to *c6pvmkl* in XSPEC but uses the *apec* collisional plasma

model for the X-ray spectrum at given plasma temperature. We note that the line broadening is self-consistently calculated in the CSW model and for the spectrum of WR 147S we adopted Gaussian broadening using the *gsmooth* model in XSPEC.

We fitted simultaneously four HETG first-order spectra of WR 147 : MEG(+1), MEG(−1), HEG(+1), HEG(−1); and two zeroth-order (undispersed) spectra: one for WR 147N and WR 147S , respectively. Table 2 and Figures 5 and 6 show the corresponding fit results. The following results are worth noting. We see that there is a good correspondence between the derived abundances from the models that assume CIE plasma or NEI shocks are responsible for the X-ray emission of WR 147S . The total observed X-ray flux of WR 147 from the *Chandra* HETG is 1.31×10^{-12} ergs cm^{-2} s^{-1} which is $\sim 12\%$ smaller than that from the *XMM-Newton* observation in November 2004 (Skinner et al. 2007). We believe that this difference is due to the calibration uncertainties between the two telescopes but the 15.48-day X-ray variability of WR 147S (see Fig. 3) may also contribute some part of it. Note that the flux value from HETG is the average X-ray flux over the proposed variability period while the *XMM-Newton* data provide a 'snap-shot' X-ray spectrum of WR 147 . Despite the fact that we adopted an average line broadening for the WR 147S spectrum, the derived value (FWHM) from the global fits is in agreement with the results from the fits to individual lines (see Table 1). But perhaps the most interesting and robust result from the global fits is that all the adopted models require very hot plasma to be present in WR 147S (Fig. 6). We mention that the hot plasma (CIE or NEI) at temperatures kT > 3 keV supplies $\sim 56-63\%$ of the total observed flux from WR 147S .

Finally, we note that we have run two more cases of the global spectral models that have orbital inclination and azimuthal angle fixed correspondingly to: (i) $i = 10^\circ$ and $\omega = 170^\circ$; (ii) $i = 50^\circ$ and $\omega = 174^\circ$. Their results are consistent with those in Table 2 and Figures 5 and 6 of our basic case with $i = 30^\circ$ and $\omega = 171^\circ$.

7. Discussion

Based on the zeroth-order data (Zhekov & Park 2010) and the analysis of the first-order spectra presented in this study, we have argued that the northern X-ray source, WR 147N , is likely associated with the CSW region of the WR 147 binary system, while we speculated that the X-ray emission of its southern counterpart, WR 147S , is likely due to stellar wind shocking onto a close unseen companion. Next, we discuss in some detail two of the most important results related to this physical picture.

7.1. Reduced Mass-Loss Rates

As described in § 6, we reduced the mass-loss rates by a factor of 4 to calibrate the CSW X-ray luminosity to that of WR 147N . On the other hand, the amount of absorption due to the stellar wind can provide us with another estimate of this parameter. From the radial column density of the assumed 'cold' stellar wind and adopted WR 147 abundances, we derive the corresponding minimum value of the absorption column density for the X-ray source located in the wind at some distance from the star: $N_{H,wind} = 2.76 \times 10^{22} \dot{M}_5 r_{12}^{-1} V_{1000}$ cm^{-2}, where $\dot{M}_5$ is the WN8 mass loss in units of 10^{-5} M$_\odot$ yr^{-1} ; r_{12} is the distance from the star in 10^{12} cm; V_{1000} is the wind velocity in units of 1000 km s^{-1} . If the X-ray source in WR 147S is located at distance equal to the semi-major axis of the orbit of the hypothesized close companion (§ 5.2; $a = 0.33$ au $\approx 5 \times 10^{12}$ cm), we see that the minimum column density of the stellar wind is $\sim 2-3$ times larger than the value derived from the global fits (Table 2) even for the factor of 4 reduced mass-loss rate ($\dot{M}_5 = 1$). A likely explanation for such a discrepancy is that we adopted a 'cold' stellar wind absorption model in the global spectral fits, that is all the chemical elements are in their neutral state. Cold gas is an efficient X-ray absorber, so, this model underestimates the column density of the stellar wind. In reality, the stellar wind is ionized considerably, more so in vicinity of the WN8 star where the putative close companion is orbiting the primary star. This results in a higher X-ray transparency of the ionized wind. Thus, to have the same optical depth as in the case of the 'cold' wind, the ionized wind must have a larger effective column density. This can likely resolve the wind-absorption discrepancy. However, to test such an absorption model we need to know the exact ionization structure of the stellar wind. This requires a detailed modeling in the optical-UV spectral range which is beyond the scope of the present study. We only note that we find higher values for $N_{H,wind}$ from the fits, with no deterioration of their quality, if we enforce a smaller column density for H, He and N, thus mimicking an appreciable deviation from neutral state for these elements. On the other hand, the important conclusion is that both the CSW luminosity and the WN8 stellar wind absorption indicate a reduced mass loss of the WN8 star by a factor of ~ 4 compared to its nominal value for WR 147 (§ 2).

From a detailed spectroscopy study of the optical-to-infrared spectrum of WR 147 , Morris et al. (2000) concluded that the clumping factor in the stellar wind of the WN8 star is in the range 0.04 to 0.25, suggesting a reduction to the mass-loss rate of 0.2 - 0.5 compared to the values derived under assumptions of wind homogeneity. Thus, if the smaller mass loss of the WN star needed to explain the X-ray data is due to wind clumping, this would mean that a considerably inhomogeneous wind extends out to large distances from the star (e.g., to the thermal radio emission region of ~ 1000 stellar radii) and only further beyond does it become homogeneous and form the CSW region of WR 147 .

But an alternative and interesting explanation can be proposed as well. A homogeneous stellar wind can have a smaller mass-loss rate, provided the distance to WR 147 is less than the currently adopted value. We note that for the mass-loss values derived from the radio observations $\dot{M} \propto d^{1.5}$ (Panagia & Felli 1975; Wright & Barlow 1975). It is worth noting that the distance to WR 147 may bear some appreciable uncertainties since it was derived by Churchwell et al. (1992) from comparative NIR photometry with the only known galactic WN8 star (WR 105) which is a member of an association and WR 105 is now re-classified as a WN9h star (van der Hucht 2001). Moreover, due to the appreciable uncertainties in the spectral type of the OB companion, Lèpine et al. (2001) pointed out another discrepancy related to the optical emission from WR 147 : either the WR star is too bright (by 1.5 mag) or its OB companion is too faint (by 1.5 mag) for their respective spectral types. We believe that future spatially resolved observations of WR 147 in the optical can help us obtain an accurate distance to this object based on a well-constrained spectral type and luminosity class of the OB companion in the binary system. In turn, the mass-loss rate of the WN8 star will be constrained better which could help us reveal the importance of clumpiness in the stellar wind at large distances from the star. Also, a well-constrained luminosity of the OB star will result in a better estimate of its X-ray luminosity, using the L_X - L_{bol} relation for hot massive stars. Consequently, we will have a more realistic value for the contribution from the OB star to the total X-ray emission of WR 147N . Note that the higher the L_X of the OB star, the higher its contribution to the X-ray emission of WR 147N , thus, the higher the mass-loss reduction required. And all this may allow us build a self-consistent physical picture of the CSW binary WR 147 .

7.2. High Plasma Temperature in WR 147S

The presence of very hot plasma (kT ~ 4 keV; Fig. 6) in the X-ray emission region of the WN8 star (WR 147S) is a result that does not depend on the accuracy of the distance to the observed object. We recall that in the framework of the CSW model the shape of the X-ray spectrum of WR 147N is well matched using the currently accepted values for the wind velocities (§ 2). But the high plasma temperature in WR 147S poses some problems for the WR 147S emission model: X-rays from stellar wind shocking onto a close companion. Given the chemical composition of the WN8 wind (Table 2), the temperature of the shocked plasma is $kT_{sh} = 2.27 V_{1000}^2$ keV, where V_{1000} is the shock velocity in units of 1000 km s^{-1} . Thus, the maximum temperature we can get for $V_{wind} = 950$ km s^{-1} is considerably smaller than that derived from the global spectral fits.

We think that one way to resolve this problem could be the following. In the adopted

scenario of X-rays from a stellar wind shocking onto a close (normal star) companion, apart from its own velocity the WN8 wind gets additionally accelerated by the gravitational field of the normal star. Qualitatively, we can assume that near the surface of the close companion the effective velocity of the WN wind is: $\mathrm{V}^2_{eff} = \mathrm{V}^2_{wind} + V^2_G$, where $\mathrm{V}^2_G = 2GM_{CO}/R_{CO}$; G is the gravitational constant; M_{CO} and R_{CO} are the companion mass and radius, respectively. In such a case, a value of $\mathrm{V}_G = 930$ km s^{-1} is required to match a plasma postshock temperature of ~ 4 keV.

To model the X-ray emission from WR 147S , we adopted two limiting cases of hot plasma distribution: (i) collisional plasma with equilibrium ionization; (ii) plasma in adiabatic shocks with non-equilibrium ionization (§ 6). Zhekov (2007) discussed the NEI effects in colliding stellar wind shocks in some detail and introduced a dimensionless parameter Γ_{NEI}. This parameter is a measure of whether or not the NEI effects are important: if $\Gamma_{NEI} \leq 1$ they must be taken into account; and they can be neglected if $\Gamma_{NEI} \gg 1$. For the scenario of the X-rays from stellar wind shocking onto a close companion, adopted here for WR 147S , we have $\Gamma_{NEI} \gg 1$ for the stellar wind parameters of WR 147 (even with the reduced mass-loss rates) and the semi-major axis of the companion orbit of $a = 0.33$ au.

Similarly, we can introduce a dimensionless parameter that can be an indicator of whether the X-ray emitting plasma is associated with adiabatic or radiative shocks. Namely, $\Gamma_{cool} = t_{flow}/t_{cool}$, where $t_{flow} = r/V_{wind}$ and $t_{cool} = \frac{3}{2}\frac{nkT}{\Lambda_{cool}}$, ($\Lambda_{cool}$ is the cooling function for collisionally ionized optically-thin plasma). Note that if $\Gamma_{cool} \ll 1$ the shocks are adiabatic while values of $\Gamma_{cool} \geq 1$ indicate radiative shocks. If for simplicity we assume that the cooling is due only to bremsstrahlung emission (which gives a lower limit to the cooling, thus, an upper limit to t_{cool}), for helium dominated plasma with stellar wind parameters $\dot{M} = 10^{-5}$ M$_\odot$ yr^{-1} , $\mathrm{V}_{wind} = 950$ km s^{-1} and orbital radius of the close companion $a = 0.33$ au, the dimensionless parameter becomes: $\Gamma_{cool} = 3.64 T^{-0.5}_{keV}$, where T_{keV} is the plasma temperature in keV. From this and Fig. 6 we see that $\Gamma_{cool} \geq 1$ for the X-ray plasma in WR 147S .

Thus, in the framework of the adopted X-ray production mechanism of stellar wind shocking onto a close companion, the values of $\Gamma_{NEI} \gg 1$ and $\Gamma_{cool} \geq 1$ indicate that X-ray emission from a distribution of CIE plasma is a more appropriate physical model for the X-ray spectra of WR 147S .

In such a case and since the shocks are radiative, we have an upper limit on the available energy (luminosity) that can be converted into X-ray emission: no more energy is emitted than the energy flux crossing the shock front per unit area. Taking into account the additional acceleration of the wind in the gravitational field of the close companion (see above), we have: $\mathrm{L}_X = \frac{1}{2}\int \rho \left(V_{wind,\perp} + V_G\right)^3 dS$ (ρ is the density of the wind in front of the shock; $V_{wind,\perp}$ is

the wind velocity component perpendicular to the shock front; S is the shock surface). For radiative shocks, the corresponding shock surface follows the shape of the stellar surface and we derive: $\mathrm{L}_X = \frac{1}{8}\left(\frac{R_{CO}}{a}\right)^2 L_{wind}\left[1+3\left(\frac{V_G}{V_{wind}}\right)+3\left(\frac{V_G}{V_{wind}}\right)^2\right]$, where $L_{wind} = \frac{1}{2}\dot{M}V_{wind}^2$ is the mechanical luminosity of the WN8 wind. Note that this is similar to eq.(80) in Usov (1992) but with a correction factor for the gravity of the companion star. And, the simple considerations presented here allow us to further check the consistency of the adopted physical picture. For a distance of 630 pc to WR 147 and the value of unabsorbed X-ray flux derived for WR 147S (Table 2), we have $\mathrm{L}_X = 1.25\times10^{33}$ ergs s^{-1}. Adopting the values of $\dot{M} = 10^{-5}$, $V_{wind} = 950$ km s^{-1} , $a = 0.33$ au and $V_G = 930$ km s^{-1} (for the latter see above), we derive $R_{CO} = 1.6$ R$_\odot$ and in turn we use the value of V_G to derive $M_{CO} = 3.6$ M$_\odot$. Thus, we see that the physical characteristics of the putative close companion of the WN8 star in WR 147 are consistent with those of an AB main sequence star (Allen 1973). Note that the mass and radius of the companion star will be smaller, provided WR 147 is located closer to us than it is currently assumed (it can be shown that in the picture described above $R_{CO}, M_{CO} \propto d^{0.25}$).

It is important to emphasize that the quantitative estimates presented here serve only as a check on the global consistency of the physical picture we speculated about in the case of WR 147S and they do not represent a detailed physical model. Nevertheless, two other results deserve a brief discussion in the framework of the adopted physical picture.

If the X-rays from WR 147S originate from a region close to the unseen and much cooler companion (therefore, *not a strong source* of far UV photons) of the main WN8 star, this may qualitatively explain why we do not find suppressed forbidden line in the helium-like triplets of Si XIII and S XV. We note that the forbidden and intercombination lines in these line complexes have intensities that are within $(1-2)\sigma$ of their nominal values (see Table 1 and compare with the *Chandra* ATOMDB). This fact seems to be in accord with the conclusion above that the emission of CEI plasma is a more appropriate model for the X-ray spectrum of WR 147S . But, if much better grating data for this source become available in the future and they reveal enhanced emission for the forbidden line in Si XIII and/or S XV, then this will pose a problem for the physical picture adopted here for the X-ray emission from WR 147S .

Grating data with very high quality are also needed to study possible variations of the line centroids in the X-ray spectrum of WR 147S . Such variations are expected with the proposed orbital period of the unseen companion if its orbit is not seen pole-on from an observer. For the data at hand, we can analyze in detail only the integrated over the orbital period X-ray spectrum of WR 147S . Thus, we can speculate that the derived line centroids being consistent with zero line shifts (see §4) may simply indicate that the axis of the orbital

plane of the unseen companion in WR 147S (the hypothesized third star in the system) is almost along our line of sight.

Finally, it is worth noting that the X-ray emission from WR 147S (the WN8 star in the WR 147 binary system) shares common characteristics with that of presumably single WN stars detected in X-rays (Skinner et al. 2010): their spectra are rather hard and a hot plasma with $kT > 2$ keV must be present in the X-ray emission region. This could be a sign that similar mechanism for X-ray production operates in all these objects. If we assume that this common mechanism is identified as a stellar wind shocking onto a close companion, then the simple considerations presented above would suggest that a $L_X \propto L_{wind}$ relation might exist for these WN stars as well. Interestingly, Skinner et al. (2010) found such a trend which, despite the appreciable scatter in the data, is stronger than that for the commonly adopted relation between the X-ray and bolometric luminosity in massive stars (e.g., compare their Figs. 9 and 10). We note that such a scatter might simply indicate various companion radii and orbital separation in different WN stars. However, it should be kept in mind that we need additional pieces of evidence for the presence of a close companion (supposedly a normal star) that would come from future X-ray observations (e.g., revealing periodic variability) or from observations in other spectral domains (e.g, see the end of § 5.2). The physical picture will be on even more solid ground if objects with similar characteristics in the X-rays are found amongst supposedly single objects of the other types of Wolf-Rayet stars (WC and WO). And we note that an WO object with hard X-ray emission is already detected: a presumably single WO star WR 142 (Oskinova et al. 2009; Sokal et al. 2010).

8. Conclusions

In this work, we presented the second part of our analysis of the *Chandra* HETG data of the WR+OB binary system WR 147 which was resolved into a double X-ray source in the zeroth-order HETG images (Zhekov & Park 2010). The basic results and conclusions are as follows:

1. Profiles of the strong emission lines in the positive and negative first-order MEG and HEG spectra were modeled simultaneously. The results are consistent with the X-ray emission coming from two sources spatially separated by $0\farcs603^{+0.10}_{-0.08}$. This value is in very good correspondence with the results from the analysis of the zeroth-order image (Zhekov & Park 2010).

2. The line profile analysis showed that the centroids of the lines in the spectrum of WR 147N are *blue-shifted* and we find no indication of suppressed forbidden lines in

the He-like triplets either in the WR 147N or in the WR 147S spectra. The latter means that in both sources: (i) the X-ray plasma is not located very close to strong UV sources, and (ii) densities in the X-ray plasma do not significantly exceed the critical density.

3. Our deep *Chandra* observations that span a period of about two weeks show that the southern source in the binary, WR 147S , exhibits X-ray variability with a period of 15.48 ± 1.91 days and a 13% amplitude with respect to its average flux.

4. The northern X-ray source, WR 147N , is probably associated with the CSW region in the wide WR+OB binary system with orbital inclination $i = 30°[0° - 60°]$. The (variable) X-rays of its southern counterpart, WR 147S (the WN8 star), likely result from the WN8 star wind shocking onto a close companion (a hypothesized third star in the system).

5. Global spectral models having two components, X-ray emission from NEI CSW hydrodynamic models for WR 147N and optically-thin plasma spectra of a distribution of hot plasma for WR 147S , provide a good match to the entire set of HETG (first and zeroth-order) spectra. We note that, first, a factor of 4 reduction of the stellar mass-loss rate relative to currently accepted values is required to match the X-ray luminosity of WR 147N . Second, very hot plasma (kT $\sim$ 4 keV) must be present in WR 147S . Note that the velocity of the WN-star wind is not high enough to provide such a postshock temperature. Thus, we propose that the higher velocity value is due to the additional wind acceleration in the gravitational field of the close companion.

This work was supported by NASA through Chandra grant GO9-0013A to the University of Colorado at Boulder, and through grant G09-0013B to the Pennsylvania State University. The authors thank an anonymous referee for her/his comments and suggestions.

Facilities: CXO (HETG, ACIS).

REFERENCES

Abbott D.C., Bieging J.H., Churchwell E., Torres A.V. 1986, ApJ, 303, 239

Allen, C.W. 1973, Astrophysical Quantities, University of London, The Athlone Press

Anders E., Grevesse N., 1989, Geochimica et Cosmochimica Acta, 53, 197

Arnaud, K.A. 1996, in Jacoby G., Barnes, J. eds., ASP Conf. Ser. Vol. 101, Astronomical Data Analysis Software and Systems, Astron. Soc. Pac., San Francisco, 17

Babel, J. & Montmerle, T. 1997, ApJ, 485, L29

Caillault, J.-P., Chanan, G. A., Helfand, D. J., Patterson, J., Nousek, J. A., Takalo, L. O., Bothun, G. D., Becker, R. H. 1985, Nature, 313, 376

Cherepashchuk, A.M. 1976, Soviet Astronomy Letters, 2, 138

Churchwell E., Bieging J.H., van der Hucht K.A., Williams P.M., Spoelstra T.A.Th., Abbott D.C. 1992, ApJ, 393, 329

Cohen, D.H., de Messieres, G.E., Macfarlane, J.J., Miller, N.A., Cassinelli, J.P., Owocki, S.P., & Liedahl, D.A. 2003, ApJ, 586, 495

Contreras M.E., Rodriguez L.F., Gomez Y., Velazquez A. 1996 , ApJ, 469, 329

Contreras M.E., Rodriguez L.F. 1999, ApJ, 515, 762

Dougherty, S.M., & Williams, P.M. 2000, MNRAS, 319, 1005

Dougherty, S.M., Pittard, J.M., Kasian, L., Coker, R.F., Williams, P.M. & Lloyd, H.M., 2003, A&A, 409, 217

Gagné, M., Oksala, M.E., Cohen, D.H., Tonnesen, S.K., ud-Doula, A., Owocki, S.P. Townsend, R.H.D., & MacFarlane, J.J. 2005, ApJ, 628, 986

Gorenstein, P. 1975, ApJ, 198, 95

Güdel M. & Nazé Y. 2009, The Astronomy and Astrophysics Review, 17, 309

Hatchett, S. & McCray, R. 1977, ApJ, 211, 552

Lebedev, M.G. & Myasnikov, A.V. 1990, Fluid Dynamics, 25, 629

Lèpine, S., Wallace, D., Shara, M.M., Moffat, A.F.J., & Niemela, V.S. 2001, AJ, 122, 3407

Luo, D., McCray R., & Mac Low, M.-M. 1990, ApJ, 362, 267

Moran J.P., Davis R.J., Spencer R.E., Bode M.F., Taylor A. R. 1989, Nature, 340, 449

Morris, P.W., van der Hucht, K.A., Crowther, P.A., Hillier, D.J., Dessart, L., Williams, P.M. & Willis, A.J. 2000, A&A, 353, 624

Myasnikov, A.V. & Zhekov, S.A. 1991, Ap&SS, 184, 287

Myasnikov, A.V. & Zhekov, S.A. 1993, MNRAS, 260, 221

Myasnikov, A.V. & Zhekov, S.A. 1998, MNRAS, 300, 686

Myasnikov, A.V., Zhekov, S.A. & Belov, N.A. 1998, MNRAS, 298, 1021

Niemela V.S., Shara M.M., Wallace D.J., Zurek D.R., Moffat A.F.J. 1998, AJ, 115, 2047

Oskinova, L.M., Hamann, W.-R., Feldmeier, A., Ignace, R. & Chu, Y.-H. 2009, ApJ, 693, L44

Panagia, N. & Felli, M. 1975, A&A, 39, 1.

Pittard J.M., Stevens I.R., Williams P.M., et al. 2002, A&A, 388, 335

Pittard J.M., Dougherty, S.M., Coker, R.F., O'Conner E.O. & Bolingbroke, N.J. 2006, A&A, 446, 1001

Pollock, A. 1987, ApJ, 320, 283

Prilutskii, O.F & Usov, V.V. 1976, Soviet Astronomy, 20, 2

Schulz, N.S., Canizares, C., Huenemoerder, D., & Tibbets, K. 2003, ApJ, 595, 365

Skinner S.L., Itoh M., Nagase F., Zhekov S.A. 1999, ApJ, 524, 394

Skinner S.L., Zhekov S.A., Güdel M., Schmutz W. 2002a, ApJ, 572, 477

Skinner S.L., Zhekov S.A., Güdel M., Schmutz W. 2002b, ApJ, 579, 764

Skinner S.L., Zhekov S.A., Güdel M., Schmutz W. 2007, MNRAS, 378, 1491

Skinner S.L., Zhekov S.A., Güdel M., Schmutz W. & Sokal, K.R. 2010, AJ, 139, 825

Sokal, K.R., Skinner S.L., Zhekov S.A., Güdel M. & Schmutz W. 2010, ApJ, 715, 1327

Stevens, I.R., Blondin, J.M. & Pollock, A.M.T. 1992, ApJ, 386, 265

ud-Doula, A. & Owocki, S.P. 2002, ApJ, 576, 413

Usov, V.V. 1992, ApJ, 389, 635

van der Hucht, K.A. 2001, New Astronomy Rev., 45, 135

Walder, R. & Folini, D. 2000, ApSS, 274, 343

Williams P.M., Dougherty S.M., Davis R.J., van der Hucht K.A., Bode M.F., Setia Gunawan D.Y.A. 1997, MNRAS, 289, 10

Wojdowski, P.S. & Schulz, N.S. 2005, ApJ, 627, 953

Wright, A.E. & Barlow, M.J. 1975, MNRAS, 170, 41

Zhekov S.A. 2007, MNRAS, 382, 886

Zhekov S.A., McCray , R., Dewey, D., Canizares, C.R., Borkowski, K.J., Burrows, D.N. & Park, S. 2009, ApJ, 692, 1190

Zhekov S.A., & Palla, F. 2007, MNRAS, 382, 1124

Zhekov S.A., & Park, S. 2010, ApJ, 709, L119

Zhekov, S.A. & Skinner, S.L. 2000, ApJ, 538, 808

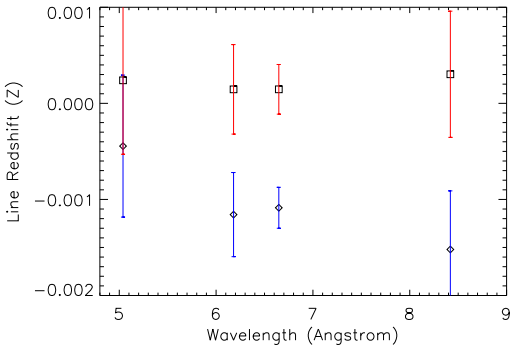

Fig. 1.— Line shifts of S XV (5.04Å), Si XIV (6.18Å), Si XIII (6.65Å) and Mg XII (8.42Å) in the total MEG/HEG(+1) and (−1) spectra. The results for the positive, $z(+1)$, and negative, $z(-1)$, arm are correspondingly denoted by diamonds (with error bars in blue) and squares (with error bars in red). For each line, the MEG and HEG data were fitted simultaneously.

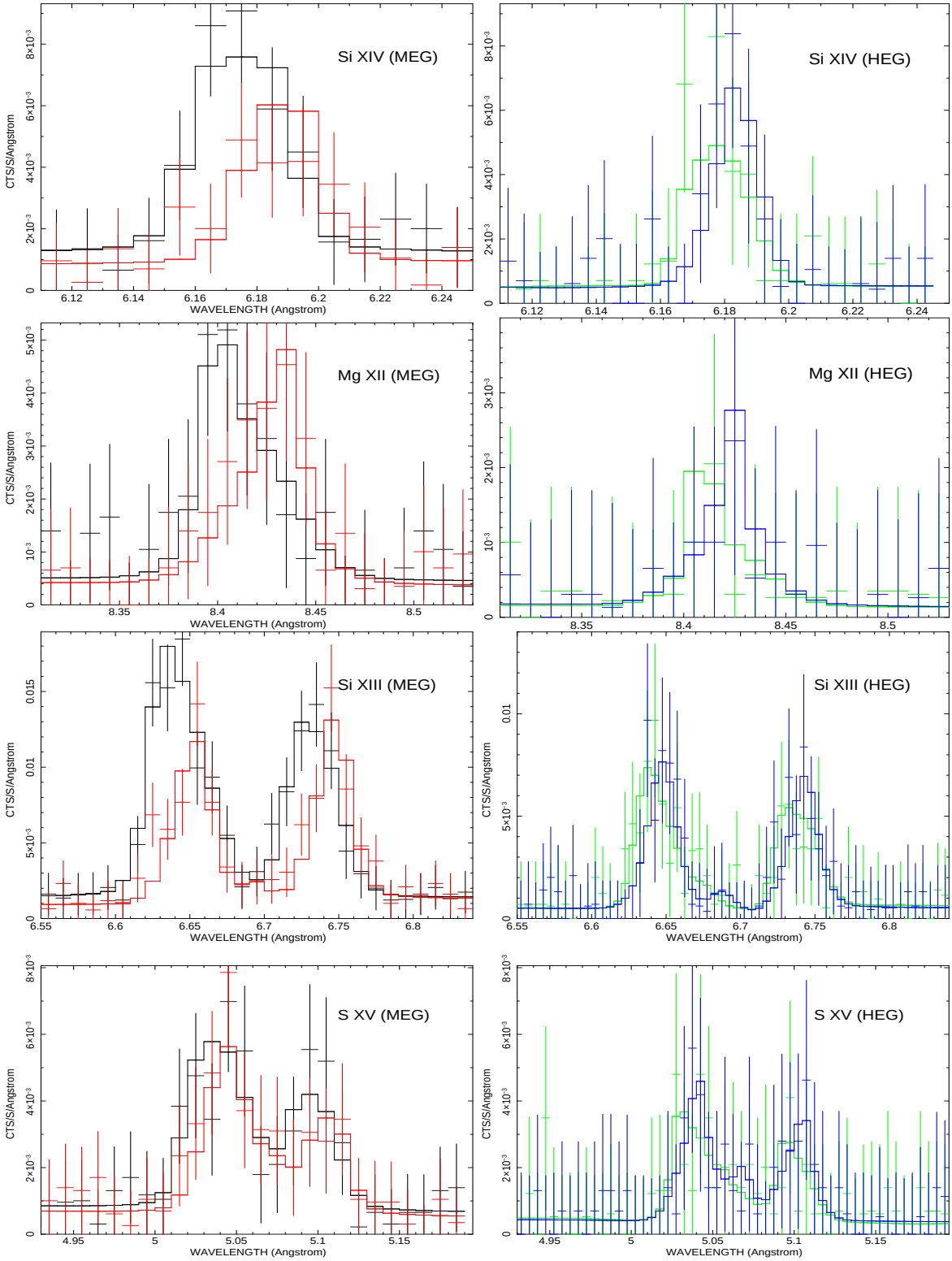

Fig. 2.— Line profile fits with the two-component model. *Left panel* shows the MEG(+1) in black and the MEG(−1) in red. *Right panel* shows the HEG(+1) in green and the HEG(−1) in blue.

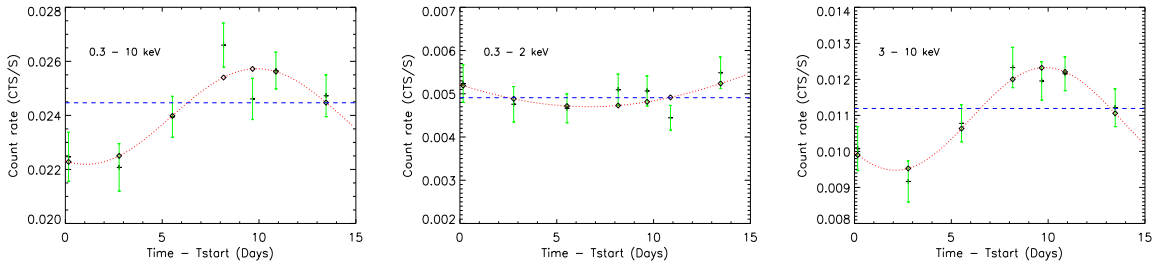

Fig. 3.— The zeroth-order background-subtracted light curves of WR 147 : the seven data points correspond to the average count rate for each observation (the data for ObsIDs 10897 and 10678 were combined, since this is one observation split into two parts). The constant-flux fit is presented by the dashed line and the fit with simple sinusoidal curve is given by the dotted line. The time (x-axis) is in days and is with respect to the start of the first observation in the HETG data set.

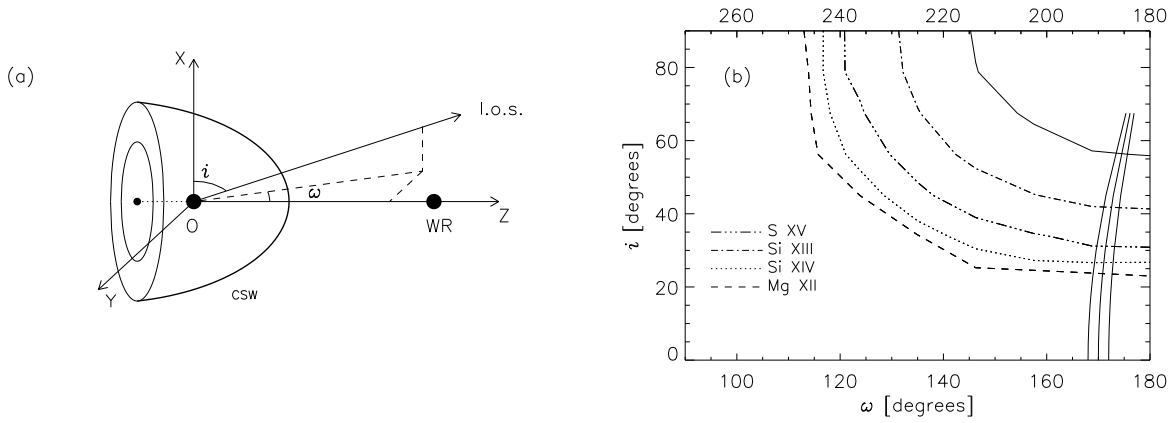

Fig. 4.— Line shifts of spectral lines that originate in the colliding stellar wind region. *Panel (a)* shows a schematic diagram of the stellar wind interaction in a WR+O binary system. The wind interaction cone is denoted by CSW (the axis Z is its axis of symmetry; the axis X is perpendicular to the orbital plane; the axis Y completes the right-handed coordinate system); the line of sight towards observer by l.o.s.; and the two related angles, i (orbital inclination) and ω (azimuthal angle) are marked as well. *Panel (b)* shows the isolines for the observed line shifts for various strong spectral lines (Table 1) on the grid of theoretical CSW models with the same stellar wind parameters but for different values of the inclination and azimuthal angles. The isoline shown with the solid line gives the upper limit to the line shifts. The three vertical solid lines correspond to the observed position angle of the WR-O star axis on the sky (the PA value $\pm 1\sigma$ error; Niemela et al. 1998).

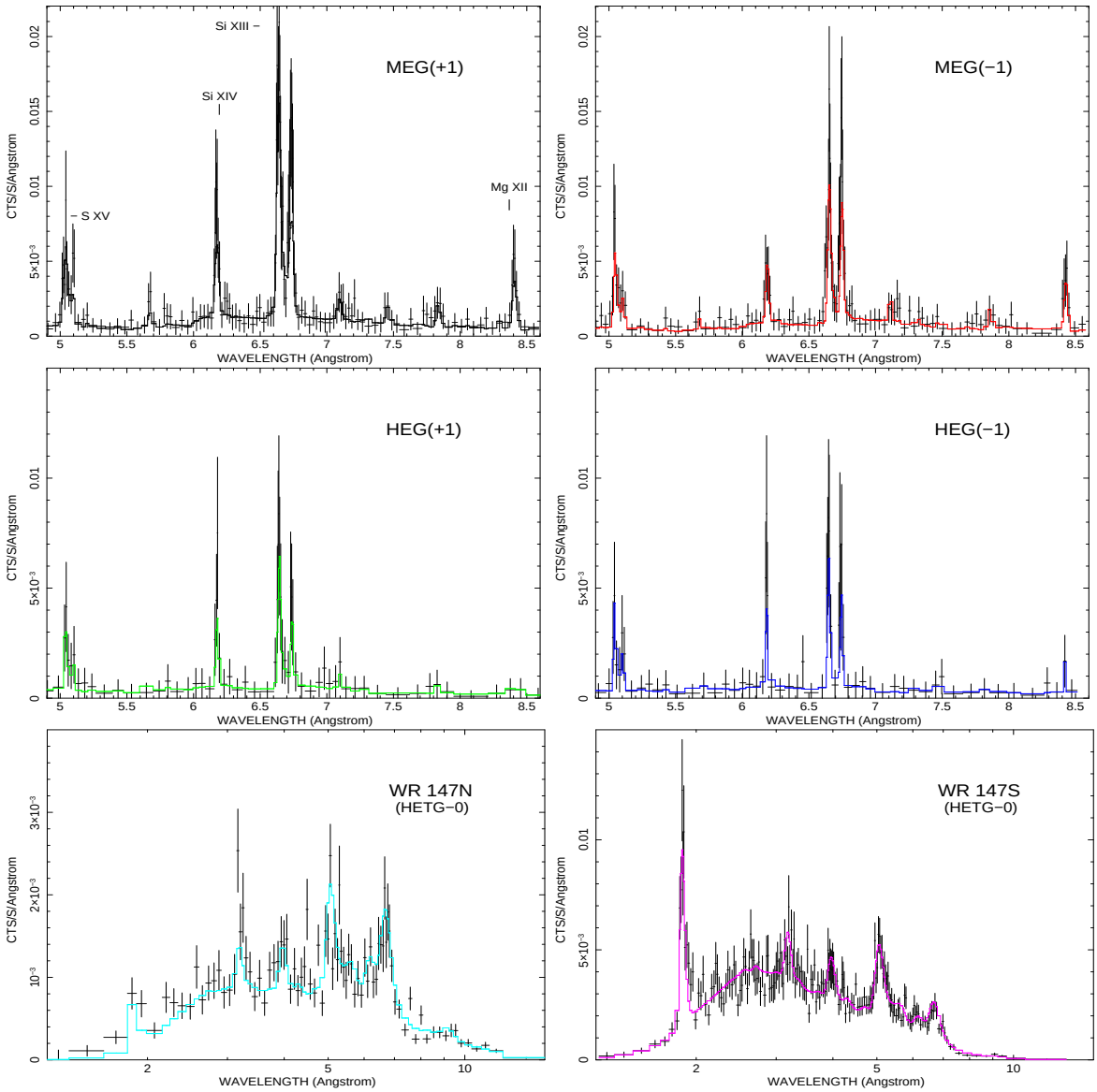

Fig. 5.— HETG background-subtracted spectra of WR 147 and the two-component model fit (Table 2 and Fig. 6). The first and zeroth order spectra were re-binned to have minimum 10 and 20 counts per bin, respectively.

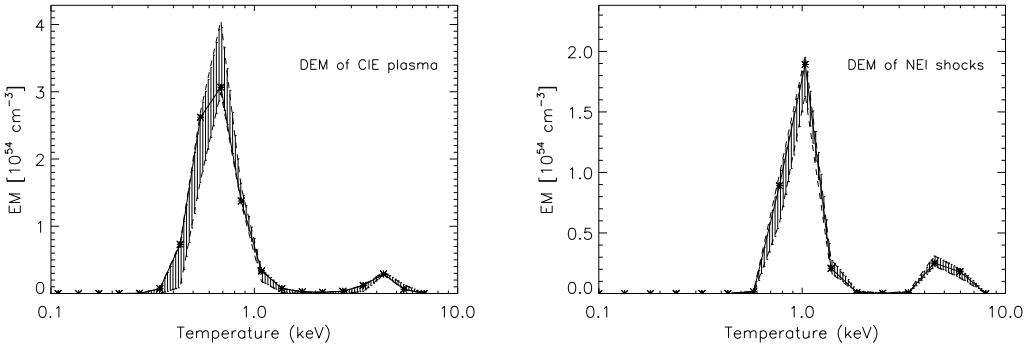

Fig. 6.— Emission measure (EM) of the WR 147S distribution of thermal plasma in collisional ionization equilibrium (DEM of CIE plasma) and of adiabatic shock with non-equilibrium ionization effects taken into account (DEM of NEI shocks). The shaded area represents 1σ errors from the fits. The EM values are for adopted distance of 630 pc to WR 147 .

Table 1. Line Parameters

Line	λ^a_{lab} (Å)	WR 147S FWHM^b (km s^{-1})	WR 147S Flux^c	WR 147N FWHM^b (km s^{-1})	WR 147N Flux^c	Line Shift^d (km s^{-1})	Δ^e (arcsec)
S XV K_α	5.0387	1300^{+395}_{-265}	$15.36^{+1.92}_{-1.92}$	< 500	$3.84^{+0.48}_{-0.48}$	-152^{+16}_{-283}	$0\farcs54^{+0.13}_{-0.14}$
(i/r)^f			$0.32^{+0.17}_{-0.14}$		0.32		
(f/r)^f			$0.67^{+0.20}_{-0.14}$		0.67		
Si XIV L_α	6.1804	665^{+450}_{-300}	$2.94^{+0.51}_{-0.78}$	< 1050	$1.62^{+0.65}_{-0.44}$	-140^{+180}_{-80}	$0\farcs66^{+0.22}_{-0.25}$
Si XIII K_α	6.6479	1200^{+225}_{-185}	$11.43^{+2.03}_{-2.66}$	670^{+261}_{-254}	$7.84^{+2.88}_{-1.80}$	-246^{+68}_{-68}	$0\farcs54^{+0.10}_{-0.13}$
(i/r)			$0.04^{+0.08}_{-0.04}$		$0.22^{+0.17}_{-0.16}$		
(f/r)			$0.75^{+0.20}_{-0.17}$		$0.66^{+0.28}_{-0.19}$		
Mg XII L_α	8.4192	1550^{+680}_{-600}	$2.04^{+0.84}_{-0.79}$	< 1500	$1.15^{+0.50}_{-0.49}$	-150^{+167}_{-107}	$0\farcs67^{+0.27}_{-0.09}$

Note. — Results from simultaneous fits to the line profiles in the MEG and HEG $(+1/-1)$ spectra with the associated 1σ errors. For the He-like triplets, the ratios of the intercombination to the resonance line (i/r) and of the forbidden to the resonance line (f/r) are given as well.

[a]The laboratory wavelength of the main component.

[b]The line width (full width at the half maximum).

[c]The observed total line/multiplet flux in units of 10^{-6} photons cm^{-2} s^{-1}.

[d]The line shift of the WR 147N component. Note that a negative velocity corresponds to a blueshift.

[e]The spatial offset between the two sources (WR 147N and WR 147S).

[f]Due to the quality of the data, it was assumed that the (i/r) and (f/r) ratios were the same in the spectra of WR 147N and WR 147S .

Table 2. Global Spectral Model Results

	CIE Plasma	NEI Shocks
χ^2/dof	561/993	526/992
$N_{H,ISM}{}^a$	2.3	2.3
$N_{H,wind}{}^a$	$0.23^{+0.01}_{-0.01}$	$0.19^{+0.01}_{-0.01}$
Ne	$0.0^{+2.7}_{-0.0}$	$1.3^{+1.6}_{-1.3}$
Mg	$4.1^{+0.9}_{-0.8}$	$3.3^{+0.5}_{-0.5}$
Si	$3.8^{+0.7}_{-0.3}$	$3.5^{+0.2}_{-0.2}$
S	$6.1^{+0.7}_{-0.7}$	$5.5^{+0.4}_{-0.4}$
Ar	$11.6^{+2.8}_{-2.8}$	$8.7^{+1.3}_{-1.3}$
Ca	$19.4^{+5.4}_{-5.3}$	$12.6^{+2.4}_{-2.4}$
Fe	$6.6^{+0.8}_{-0.9}$	$7.7^{+0.6}_{-0.6}$
FWHM^b	840^{+400}_{-220}	1000^{+100}_{-260}
τ^c		$1.03^{+0.17}_{-0.12}$
$F_{X,\ WR\ 147N}{}^c$	0.327 (9.5)	0.326 (10.1)
$F_{X,\ WR\ 147S}{}^c$	0.975 (26.3)	0.992 (28.1)

Note. — Results from simultaneous fits to the combined (WR 147N+S) first-order spectra and the individual undispersed (zeroth-order) spectra for WR 147N and WR 147S . Errors are the 1σ values from the fits. All abundances are with respect to their solar values (Anders & Grevesse 1989). The fixed in the fit abundances are: H= 1, He= 25.6, C= 0.9, N= 140, O= 0.9, and Ni= 1 (for details see Skinner et al. 2007; Zhekov 2007). The corresponding distributions of emission measure vs. electron temperature of the hot plasma are shown in Fig. 6.

[a]The X-ray absorption in units of 10^{22} cm^{-2}. Only the spectrum of WR 147S is subject to excess X-ray absorption that is due to a cold stellar wind ($N_{H,wind}$) with the same abundances as the X-ray emitting plasma.

[b]The average full width of half maximum for the lines in the spectrum of WR 147S . Units are km s^{-1} .

[c]The ionization age ($n_e t$) of the shocks in units of 10^{11} cm^{-3} s.

[d]The observed X-ray flux (0.5 - 10 keV) followed in parentheses by the unabsorbed value. Units are 10^{-12} ergs cm^{-2} s^{-1}.